Available online at www.sciencedirect.com
SCIENCE DIRECT®
PERGAMON
Polyhedron 22 (2003) 1889–1896
POLYHEDRON
www.elsevier.com/locate/poly

Environmental factors influencing EPR in Mn_{12}-Ac and Fe_8Br

S. Hill [a,*], R.S. Edwards [a], J.M. North [b], K. Park [b,1], N.S. Dalal [b]

[a] Department of Physics, University of Florida, Gainesville, FL 32611-8440, USA
[b] Department of Chemistry and Biochemistry and NHMFL, Florida State University, Tallahassee, FL 32310, USA

Received 6 October 2002; accepted 12 January 2003

Abstract

A multi-high-frequency (40–200 GHz) resonant cavity perturbation technique yields distortion-free high-field EPR spectra for oriented single crystal samples of the uniaxial and biaxial spin $S = 10$ single molecule magnets (SMMs) Mn_{12}-Ac and Fe_8Br. We examine quantitatively the temperature dependence of the EPR linewidths and line shifts for fixed frequency measurements with an applied magnetic field along the easy axis. Simulations of the obtained experimental data take into account various environmental couplings, including intermolecular spin–spin interactions (dipolar and exchange), as well as distributions in the zero-field crystal field parameters. The temperature dependence of the linewidths and the line shifts are mainly caused by spin–spin interactions. For Fe_8Br and Mn_{12}-Ac, the calculated line shifts and linewidths agree well with the observed experimental trends. The linewidths for Fe_8Br reveal a stronger temperature dependence than those for Mn_{12}-Ac because, for the latter, a much wider distribution in D overshadows the temperature dependence of the spin–spin interactions. For Fe_8Br, the line-shift analysis suggests two competing interactions: a weak effective ferromagnetic exchange coupling between neighboring molecules, and a longer-range antiferromagnetic dipolar interaction. For Mn_{12}-Ac, a pronounced modulation of the EPR lineshapes for transverse applied fields suggests the possibility of a solvent-disorder-induced transverse anisotropy, as has recently been proposed by other groups. These findings could have implications for the mechanism of quantum tunneling of magnetization in both of these SMMs.

Keywords: Single molecule magnets; Nanomagnet; Electron paramagnetic resonance; Quantum tunneling; Manganese

1. Introduction

Single molecule magnets (SMMs) such as $[Fe_8O_2(OH)_{12}(tacn)_6]Br_8\cdot 9H_2O$ (Fe_8Br) and $[Mn_{12}O_{12}(CH_3COO)_{16}(H_2O)_4]\cdot 2CH_3COOH\cdot 4H_2O$ (Mn_{12}-Acetate, or Mn_{12}-Ac), have attracted considerable interest due to their novel quantum properties and their possible future use in computational devices [1,2]. Both materials may be thought of as consisting of 3D arrays of identical high-spin ($S = 10$) clusters (magnetic quantum dots) with the same magnetic properties and characteristic energies.

To lowest order, the effective spin Hamiltonian for the Mn_{12}-Ac and Fe_8Br systems has the form [1,3–7]

$$\hat{H} = D\hat{S}_z^2 + \mu_B \vec{B}\cdot\ddot{g}\cdot\hat{S} + \hat{H}' \quad (1)$$

where D (<0) is the uniaxial anisotropy constant, the second term represents the Zeeman interaction with an applied field $\vec{B}$, and $\hat{H}'$ includes higher order terms in the crystal field ($\hat{O}_2^2$, $\hat{O}_4^0$, $\hat{O}_4^2$ and $\hat{O}_4^4$, etc. [3–9]), as well as environmental couplings such as intermolecular dipolar and exchange interactions [8–11]. D is negative for both Mn_{12}-Ac (-0.454 cm^{-1} [12]) and Fe_8Br (-0.203 cm^{-1} [6]). For the strictly axial case (B//z and $\hat{H}' = 0$), the energy eigenstates may be labeled by the quantum number M_S ($-S \le M_S \le S$), which represents the projection of S on to the easy axis. In zero field, the energy eigenvalues are then given by the expression $\varepsilon = DM_S^2$, resulting in an energy barrier separating doubly degenerate ($M_S = \pm i$, $i =$ integer $\le S$) 'spin-up' and 'spin-down' states [1]. At low temperatures ($k_BT \ll DS^2$), this barrier inhibits magnetic relaxation via thermal activation; hence the potential of SMMs for magnetic memory applications. However, terms in $\hat{H}'$ that do not commute with $\hat{S}_z$ mix M_S states

* Corresponding author. Tel.: +1-352-392-5711; fax: +1-352-392-3591.
E-mail address: hill@phys.ufl.edu (S. Hill).
[1] Present address: Code 6390, Naval Research Laboratory, Washington, DC 20375, USA.

0277-5387/03/$ - see front matter
doi:10.1016/S0277-5387(03)00247-X

of either polarization, giving rise to the situation in which any given eigenstate may be made up from coherent superpositions of unperturbed states on either side of the barrier. Under these circumstances, a 'spin-up' state may evolve (quantum tunnel) with time into a 'spin-down' state [13]. Although detrimental in terms of magnetic memory applications, this process may prove useful for quantum computation [2].

Both Fe_8Br and Mn_{12}-Ac exhibit magnetic quantum tunneling (MQT) at low temperatures (<1 K) [14,15], yet the origin of this effect remains unclear. For Fe_8Br, a rhombic distortion gives rise to a term in $\hat{H}'$ of the form $E(\hat{S}_x^2-\hat{S}_y^2)$, where $E=0.032$ cm^{-1} [6,7]. Although such an interaction causes tunneling, current leading theories additionally invoke inter-SMM dipolar and nuclear hyperfine fields in order to accurately explain the observed low temperature relaxation [16]. For Mn_{12}-Ac, it has long been assumed that the rhombic term is zero due to its S_4 molecular site symmetry; for this reason, other sources of symmetry breaking are required in order to explain the MQT. While recent high-frequency EPR [3,12] and neutron studies [5] have provided convincing evidence for a fourth order single-ion transverse anisotropy ($\hat{O}_4^4$) in Mn_{12}-Ac, such an interaction cannot explain many key experimental factors associated with the observed low temperature magnetic relaxation [17,18]. For this reason, recent theoretical and experimental efforts have focused on the possible role played by disorder [8–12,18–23].

In view of the above, experimental characterizations of all possible couplings of SMMs to their environment are badly needed. This is important not only from the perspective of the mechanism for tunneling, but also for gaining deeper insights into the interactions which give rise to quantum decoherence. Any interaction contained within $\hat{H}'$ may be expected to give rise to distinct spectroscopic signatures which may be measured using single-crystal EPR [8–12]. For example, higher order terms in the crystal fields modify EPR transition energies, while other environmental couplings affect EPR lineshapes and widths. However, due to the significant axial crystal field (D) and the large spin ($S=10$), considerable zero-field energy splittings give rise to a situation in which Fe_8Br and Mn_{12}-Ac (indeed, most SMMs) are EPR silent at the low frequencies traditionally used by EPR spectroscopists. This necessitates new techniques operating above 100 GHz and, in particular, single crystal work requires high sensitivities which can only be achieved using a resonant cavity perturbation technique [24]. In this article, we review a wide body of recent single crystal EPR experiments which we have carried out on Fe_8Br and Mn_{12}-Ac. These studies highlight important new aspects of the couplings between SMMs and their environment.

2. Experimental

We use a cavity perturbation technique in combination with a broad-band Millimeter-wave Vector Network Analyzer (MVNA) exhibiting an exceptionally good signal-to-noise ratio; a detailed description of this instrumentation can be found in Ref. [24]. The MVNA/cavity combination has been shown to exhibit a sensitivity of at least 10^9 spins G^{-1} s^{-1}, which is comparable with the best narrow-band EPR spectrometers. This, coupled with newly acquired sources and a split-pair magnet, allows single crystal measurements at any frequency in the range from 8 to 250 GHz, at temperatures down to 1.2 K ($\pm$0.01 K), and for any geometrical combination of DC and AC field orientations. Further details of the experiments, and representative raw data may be found in Refs. [8–12].

All measurements were performed in the standard EPR configuration with the AC excitation field transverse to the DC field. The samples were grown using standard techniques [25,26]. All of the Fe_8Br data presented in this paper were obtained for a single sample which had an approximately rhombic shape ($1\times1\times0.2$ mm^3); the sample was aligned via in situ rotation of the cavity (containing the sample) relative to the applied field. From the angle dependence of the spectra, the orientation of the Fe_8Br sample was determined to within an accuracy of a few degrees; all of the Fe_8Br data presented in this paper are for the DC field aligned parallel to the easy axis. Three different Mn_{12}-Ac samples were used in these investigations, each having approximate dimensions $1\times0.1\times0.1$ mm^3. Easy axis data were obtained for sample A; field alignment for this sample was again achieved via in-situ rotation, with an accuracy of better than 0.3°. Hard axis Mn_{12}-Ac spectra were obtained for two samples (B and C); for these investigations, the needle shaped samples were positioned flat on the cavity end plate, thereby assuring field alignment within the hard magnetic (x, y) plane of the sample to within an accuracy of about 0.5°. For the second of these samples (C), data were obtained for two field orientations within the hard plane, corresponding to (i) alignment with one of the short edges of the sample, and (ii) at approximately 45° to this orientation, i.e. along the diagonal of the approximately square cross section of the sample.

3. Results and discussion

3.1. Easy axis spectra

Fig. 1 shows the easy axis EPR linewidths for various spin transitions (indicated in the figure) for Fe_8Br, both as a function of temperature and as a function of frequency; the inset in the lower panel of Fig. 1 shows

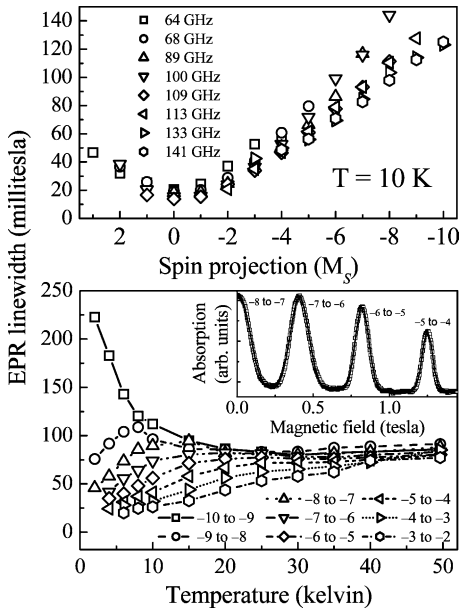

Fig. 1. Upper panel: a compilation of the M_S (level from which the transition was excited) dependence of the Gaussian EPR linewidths obtained for Fe_8Br at 10 K and at many different frequencies (indicated in the figure); see text for a discussion of the data. Lower panel: temperature dependence of the Gaussian EPR linewidths obtained for different spin transitions (indicated in the figure); the data were obtained at a frequency of 116.931 GHz, with the field applied parallel to the easy axis. The inset in the lower panel shows raw data, with the Gaussian fits superimposed.

representative raw data with Gaussian fits to the data superimposed. To begin with, the Gaussian linewidths are suggestive of an inhomogeneous broadening mechanism. Indeed, the pronounced (almost linear) increase in EPR linewidth with M_S (upper panel of Fig. 1) is due to D-strain, i.e. a distribution in D [8–10]. Since, to lowest order, the $2S+1$ quantum levels have energies proportional to M_S^2, the energy differences (i.e. EPR transition frequencies) should scale as M_S; hence D-strain produces a linear energy width ($\Delta\varepsilon$) dependence on M_S, which projects onto a width in field (ΔB) that also scales linearly with M_S. The rounding close to $M_S = 0$ is due to a convolution of the intrinsic lifetime broadening and the M_S dependent contribution [10]. The slight narrowing as a function of increasing frequency, and the weak asymmetry about $M_S = -1/2$, is due to the fact that higher (lower) frequency (M_S) transitions are observed at higher magnetic fields, where the inter-SMM dipolar broadening is weaker (see discussion below).

The temperature dependent contribution to the linewidths for Fe_8Br (lower panel of Fig. 1) is dominated by random/fluctuating intermolecular magnetic interactions *both* dipolar and, as we shall discuss below, exchange interactions [11]. At 116 GHz, the $M_S = -10$ to -9 transition occurs very close to zero-field (≈ 0.1 T). Under zero-field cooling, the spin-up ($M_S = -10$) and spin-down ($M_S = +10$) states will be equally populated. Hence, the random distribution of spin-up and spin-down molecules results in a maximal contribution to the Gaussian EPR line broadening, as evidenced by the extremely large temperature dependent contribution to the $M_S = -10$ to -9 transition in Fig. 1 as $T \rightarrow 0$ K. Upon raising the temperature, higher levels in the scheme ($|M_S| < 10$) become populated, and the individual moments begin to fluctuate more rapidly, thus leading to a suppression of the broadening. The same qualitative picture may be applied to the other transitions ($M_S = -9$ to -8 etc.), provided that k_BT exceeds the Zeeman splitting of the ground state. For k_BT less than the ground state Zeeman splitting, the system polarizes as $T \rightarrow 0$ K, and the dipole fluctuations are suppressed, leading to an EPR line narrowing, as confirmed for all but the $M_S = -10$ to -9 transition in Fig. 1. The crossover occurs when the $M_S = +10$ state starts to depopulate, i.e. approximately when $k_BT^* = g\mu_BB$. We have shown that this crossover temperature (T^*) does, indeed, scale linearly with B for all but the lowest field transition [9], thus supporting the picture of broadening due to fluctuating intermolecular interactions.

Fig. 2 shows remarkably similar trends for Mn_{12}-Ac. However, due to the larger energy scale (larger D) associated with this system, we only observe transitions at relatively high temperatures, and these are due to populations well above the ground state; the lowest

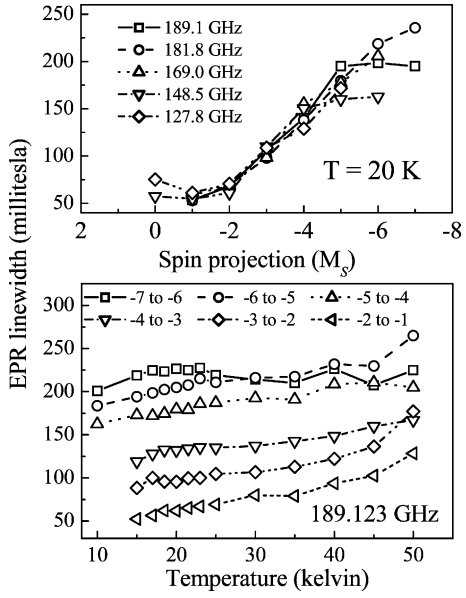

Fig. 2. Upper panel: a compilation of the M_S (level from which the transition was excited) dependence of the Gaussian EPR linewidths obtained for Mn_{12}-Ac at 20 K and at many different frequencies (indicated in the figure); see text for a discussion of the data. Lower panel: temperature dependence of the Gaussian EPR linewidths obtained for different spin transitions (indicated in the figure); the data were obtained at a frequency of 189.123 GHz, with the field applied parallel to the easy axis.

accessible transition is $M_S = -7$ to -6. Thus, when one compares the M_S dependence for both SMMs, it is apparent that the D strain in Mn_{12}-Ac is considerably stronger than for Fe_8Br; indeed, our analysis indicates a factor of ~ 3 increase in the width of the distribution in D for Mn_{12}-Ac ($\sigma_D = 1.8\%$), as compared to Fe_8Br ($\sigma_D = 0.64\%$). In addition, a weak g-strain ($\sigma_g = 0.2\%$) is found for Mn_{12}-Ac; the details of this analysis are published elsewhere [9–11]. It should be emphasized that the measured D-strains depend on sample quality, and we have noted variations from one batch of samples to another, as well as variations over time [11]. These factors are consistent with the fact that D-strain should be related to disorder in the sample; we discuss possible sources of disorder further below. The increased D-strain for Mn_{12}-Ac masks the temperature dependent contribution to the linewidths (lower panel in Fig. 2), which are rather weak in comparison to the M_S dependent contribution. In particular, no crossover in the temperature dependence is observed at low temperatures.

The upper panel of Fig. 3 shows the temperature dependent shifts in the EPR line positions obtained for Fe_8Br. When compared to Fig. 1, it is noticeable that there is a similar crossover in the temperature dependence for transitions from levels with $|M_S < 10|$. Therefore, this low temperature limiting behavior may also be attributed to a polarization of the spin system. However, long-range spin–spin (dipolar) interactions alone cannot explain the opposing temperature dependence of the

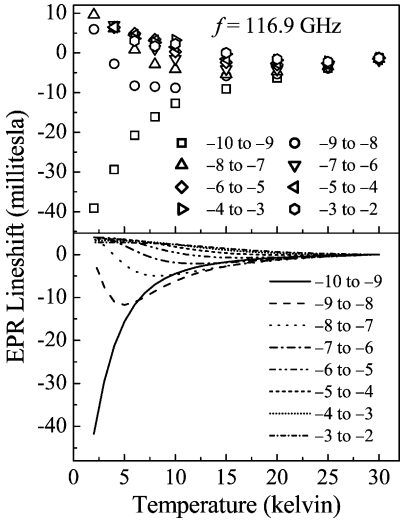

Fig. 3. Upper panel: temperature dependence of the Fe_8Br EPR line positions obtained for different spin transitions (indicated in the figure); the data were taken at a frequency of 116.931 GHz, with the field applied parallel to the easy axis. The line positions [$B(T)$] have been normalized to their positions at 30 K [B(30 K)]. Lower panel: calculated line shifts versus temperature for Fe_8Br at a frequency of 116.9 GHz; details concerning the calculations, which take into account both intermolecular dipolar and exchange interactions, can be found in Ref. [11].

$M_S = -10$ to -9 transition and the remaining $|M_S < 10|$ transitions. In order to resolve this issue, we recently demonstrated that a competition between local intermolecular exchange interactions and longer-range dipolar interactions can account for the observed trends [11]. Indeed, not only qualitative, but also quantitative agreement is found, as shown in the lower panel of Fig. 3. Many possible competing interactions have been examined, and the only combination that can account for the line shifts is a weak effective ferromagnetic exchange term ($J = -7$ G) and a longer-range antiferromagnetic dipolar coupling (~ 20 G). A detailed account of this analysis is published in Ref. [11]. These studies are the first to demonstrate significant intermolecular exchange interactions in the widely studied Fe_8Br SMM. We note that intermolecular exchange interactions have recently been studied in various other SMM systems, leading to a host of novel low temperature quantum phenomena, including exchange biasing of hysteresis loops [27–29]. Line shifts for Mn_{12}-Ac are too small to make definitive conclusions about intermolecular exchange interactions. However, a measurable dipolar contribution to the line widths is found, in addition to the considerable D- and g-strain effects [11].

3.2. Hard axis spectra

Having identified a significant D-strain effect, it is natural to search for any indications of disorder in the hard axis spectra. Indeed, hard axis data are more sensitive to the transverse interactions in $\hat{H}'$ which give rise to quantum tunneling. Cornia et al. have proposed a model in which disorder in the acetate acids of crystallization surrounding the Mn_{12} molecule gives rise to a local transverse quadratic anisotropy [20], i.e. a local rhombic distortion. Such a disorder may be expected to result in several distinct species (isomers) of Mn_{12}-Ac, each having slightly different (i.e. a distribution) tunnel splittings caused by the slightly different solvent-disorder-induced rhombic terms in $\hat{H}'$. Such a model is quite appealing, since magnetic relaxation experiments clearly indicate a distribution in the tunnel splittings for Mn_{12}-Ac [18,19]. An alternative model proposed by Garanin and Chudnovsky involves a transverse quadratic anisotropy induced via dislocations [23]; the long-range strains produced by these dislocations are predicted to result in very broad distributions of the tunnel splittings. While both disorder pictures can explain many aspects of the reported magnetic relaxation experiments, their respective spectroscopic signatures may be expected to be quite different.

Cornia et al. support their model with a set of 95 GHz EPR spectra [20]. It is argued that a splitting observed in several EPR peaks (for a field $\perp$ easy axis) is caused by two distinct Mn_{12}-Ac isomers, having different rhombic anisotropies. Meanwhile, Amigó et al. invoke similar

arguments to account for a dramatic splitting in their EPR absorption data [21], albeit their experimental findings are compared with the model of Garanin and Chudnovsky [23]. We have recently shown that the splitting observed by Amigó et al. has a very different origin, which is unrelated to distributions in the transverse anisotropy; these findings are published elsewhere [30]. Furthermore, it is unlikely that one would observe distinct absorption peaks in the case of a long-range strain-induced rhombic distortion; more likely, one would observe a broadening of the resonance linewidths, with a lineshape that reflects the distribution. It should be noted that Cornia et al. utilize a field modulation technique [20], which means that it is the derivative of the absorption that shows a splitting, not the direct absorption, i.e. the splitting is rather subtle.

The upper panel of Fig. 4 shows direct EPR absorption spectra obtained for Mn_{12}-Ac (sample B) at three different relatively low frequencies; for this sample, no special care was taken to align the magnetic field within the hard plane. The data were obtained at 1.3 K. Consequently, the strong absorption corresponds to an excitation from the ground state. As we shall show below, this transition behaves more-or-less as expected according to Eq. (1), with $S = 10$. The weak shoulder on the 77.4 GHz trace at about 8 T has a complicated origin, and is the subject of a separate publication [30]. The asymmetric lineshape is due to the non-linear Zeeman splitting of the ground state [4]. Very careful inspection of the lineshapes reveals a very subtle modulation; this is, perhaps, most visible as a shoulder on the high-field sides of the resonances. When one takes derivatives of the absorption (lower panel), the modulation of the lineshape becomes very apparent. Indeed, multiple structures are observed in the derivatives. These data may be compared to those of Cornia et al. [20], who also plot absorption derivatives. The present study reveals even more fine structure, which may have several explanations: our sample may be of a higher quality, therefore possessing less D-strain which would otherwise obscure some of the fine structure; the alignment of the field within the hard plane may be different for the two experiments; or the lower temperature of these experiments may lead to an improved resolution.

In the light of possible differences between the data in Fig. 4 and those in Ref. [20], we set about a more systematic investigation of this possible solvent-disorder effect. Fig. 5 shows derivatives of the hard axis absorption obtained for Mn_{12}-Ac sample C. The two traces obtained at each frequency correspond to two field orientations within the hard (x, y) magnetic plane of the sample; the reason for this choice will become clear below. Without detailed information concerning the fourfold magnetic axes of the sample, we chose directions relative to the well defined crystal faces, i.e. parallel to one of the short edges ($\phi = 45°$) and at 45° to this direction ($\phi = 0°$), as shown in the inset to Fig. 5. The assignments of the angle ϕ are tentatively based on the ensuing discussion of the data. The differences for the two orientations are quite remarkable, and require considerable explanation. First of all, the strongest

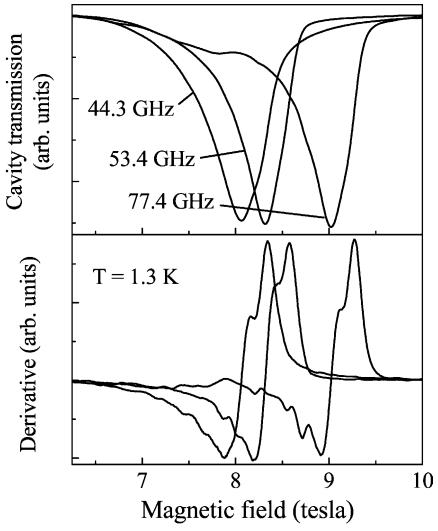

Fig. 4. Upper panel: low temperature hard axis EPR absorption for Mn_{12}-Ac (sample B) at three different relatively low frequencies (indicated in the figure); the broad resonance corresponds to the ground state transition. A very weak modulation of the EPR line shape becomes very apparent when one takes derivatives (lower panel). The multiple fine structures suggest a distribution of transverse crystal field parameters, possibly due to solvent-disorder, as recently suggested by Cornia et al. [20].

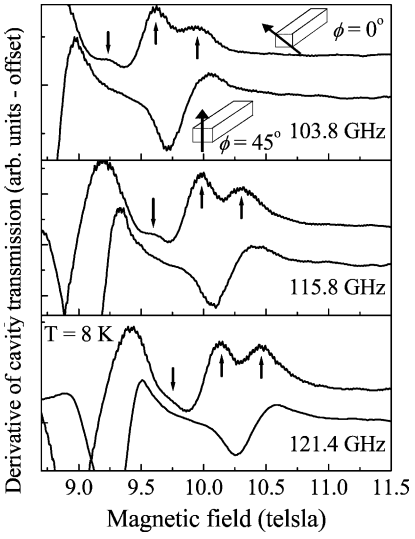

Fig. 5. Derivatives of Mn_{12}-Ac (sample C) hard axis spectra obtained at three frequencies for two different orientations of the applied field within the hard plane—$\phi = 0°$ (upper trace in each panel) and $\phi = 45°$ (lower trace in each panel); the temperature is 8 K in each case. The insets in the upper panel indicate the orientations of the applied field relative to the geometry of the sample—see main text for explanation. Splittings of the EPR peaks (indicated by arrows) are only observed for the $\phi = 0°$ data.

signals below 9.5 T in the lower panel, which move to lower fields upon lowering the frequency, correspond to an excited state transition and should be ignored for the purposes of this discussion [30]. The $\phi = 0^\circ$ data (upper traces) show several fine structures (indicated by arrows) which are similar to those in Fig. 4, albeit the spacing in the fine structure is greater for the $\phi = 0^\circ$ data in Fig. 5. Indeed, the main double peaks (indicated with up arrows) are almost identical to those observed by Cornia et al. [20], and the spacing between the double peaks of about 0.35 T also agrees. Meanwhile, this fine structure is completely absent in the $\phi = 45^\circ$ data. Two other points to note regarding the two orientations are: (i) the overall linewidth is greater for $\phi = 0^\circ$; and (ii) the points where the slopes are greatest (center of the transition) are shifted relative to each other by about 0.4 T.

Assuming that the fine structure is due to local rhombic distortions, then the ϕ dependence has a natural explanation. The quadratic term in $\hat{H}'$ has the form $\hat{S}_x^2 - \hat{S}_y^2$; this interaction produces a twofold rotation pattern for rotations in the x, y plane, with nodes at $\phi = 45$, 135°, etc. An intrinsic quadratic anisotropy would produce shifts in the hard axis EPR peaks. Depending on the sign of the interaction (sign of E), these shifts would be to higher (lower) fields at $\phi = 0$ and 180°, and to lower (higher) fields at $\phi = 90$ and 270°. However, in the case of Cornia's model (involving solvent-disorder [20]) one expects equal numbers of molecules having positive and negative E. This is because the disorder involves an acetic ligand which can take four different positions about the z-axis of the molecule. Thus, one expects overlapping twofold patterns with a 90° phase shift. Consequently, one should still expect nodes at $\phi = 45^\circ$, etc., i.e. the $\phi = 45^\circ$ spectra should be insensitive to the disorder. This explains the absence of fine structure and the sharper transitions for this orientation. On the other hand, one should see the maximum effects of the disorder-induced rhombic distortion at $\phi = 0^\circ$, i.e. splittings corresponding to the 50/50 mix of positive and negative E molecules. The observation of multiple fine structures may signify additional configurations of the acetatic ligands; all possible combinations have been discussed in detail in Ref. [20]. The lesser degree of splitting observed in Fig. 4 is most likely due to field alignment somewhere intermediate between $\phi = 0$ and 45°. The temperature dependence of the $\phi = 0^\circ$ absorption derivatives (Fig. 6) provides the final confirmation that the splitting is due to distinct ground states, presumably different solvent isomers. Both components of the splitting persist to the lowest temperatures investigated, while the intensity in all of the excited state transitions vanishes as $T \to 0$.

We conclude this section by addressing the overall shift in the spectra observed for the two orientations in Fig. 5 ($\phi = 0$ and 45°). This has a natural explanation in terms of the quartic interaction in $\hat{H}'$ ($\hat{O}_4^4$). Since this is an intrinsic crystal field term (same for all molecules), it produces shifts in the peaks with a fourfold rotation pattern within the x, y plane, with nodes at $\phi = 22.5$, 67.5°, etc. Meanwhile, at $\phi = 0$ and 45°, the shifts will be to lower and higher fields, respectively, (or vice versa). Fits to the data which take this fourth order term into consideration are discussed below.

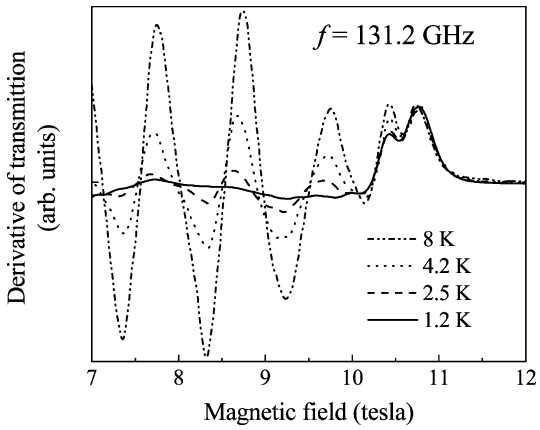

Fig. 6. Temperature dependence of the derivatives of hard axis spectra obtained for Mn_{12}-Ac (sample C) at a frequency of 131.2 GHz ($\phi = 0^\circ$). With the exception of the highest field split-peak, all of the lower field peaks vanish as $T \to 0$ K. Since all of the split-peaks seem to persist as $T \to 0$, this suggest that the splitting is caused by different ground states of the molecules. The very weak temperature dependence is probably related to the temperature dependence of the linewidths.

3.3. Fits for Mn_{12}-Ac

Fig. 7 plots the easy axis resonance positions (in field) versus frequency for sample A, along with a best fit to the data according to Eq. (1). This fit is insensitive to the transverse terms in Eq. (1), to within sensible ranges of the coefficients. Therefore, it provides an excellent constraint on the diagonal terms (D, B_4^0 and $g_{//}$) which

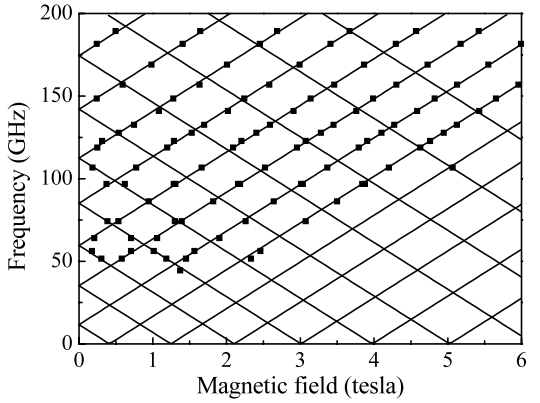

Fig. 7. Mn_{12}-Ac easy axis resonance positions (in field) versus frequency for sample A, along with a best fit to the data according to Eq. (1); the data were obtained at 20 K. The parameters obtained from the fit are listed in Table 1.

Table 1
A comparison between the Hamiltonian parameters (up to fourth order) obtained for Mn_{12}-Ac from this and other studies

	Our work (cm^{-1})	Ref. [3] (cm^{-1})	Ref. [5] (cm^{-1})
D	$-0.454(1)$	$-0.46(2)$	$-0.457(2)$
B_4^0	$-2.0(2)\times10^{-5}$	$-2.2(2)\times10^{-5}$	$-2.33(4)\times10^{-5}$
B_4^4	$\pm3\times10^{-5}$	$\pm4(1)\times10^{-5}$	$\pm3.0(5)\times10^{-5}$
$G_\parallel$	2.00	1.93(1)	–
$G_\perp$	1.94	1.96(1)	–

we then use as a basis for determining B_4^4 and $g_\perp$ from the transverse spectra. The parameters obtained from the fit are listed in Table 1. Fig. 8 shows optimum fits to the hard axis data for the two orientations in Fig. 5 ($\phi = 0$ and 45°). The fits are based on the absorption spectra, and do not take into account the disorder-induced splittings observed in Figs. 4 and 5. The low frequency data (β resonances) which deviate from the $S = 10$ fits are discussed in a separate publication [30], where it is shown that they may correspond to an $S = 9$ excited state of Mn_{12}-Ac.

All of the Hamiltonian parameters obtained from the fits in Figs. 7 and 8 are compared to powder EPR [3] and neutron [5] results in Table 1; the agreement between the various techniques is quite good. The value obtained for B_4^4 from these studies (Table 1) represents a lower bound, since we cannot be sure that the field was accurately aligned along $\phi = 0$ and 45° (the orientations that would produce the maximal shifts). Nevertheless, this value is in good agreement with other published results [3,5]. Based on the magnitudes of the splittings in Fig. 5, we can also estimate a magnitude for the disorder induced quadratic anisotropy. Surprisingly, this turns out to be quite large, on the order of 0.01 cm^{-1}. This is a factor of four or five bigger than the values calculated in Ref. [20]. However, the splittings observed in Fig. 5 are essentially identical in magnitude to those reported in Ref. [20]. The reason for the differences between our experiments and the calculated values clearly require further investigation.

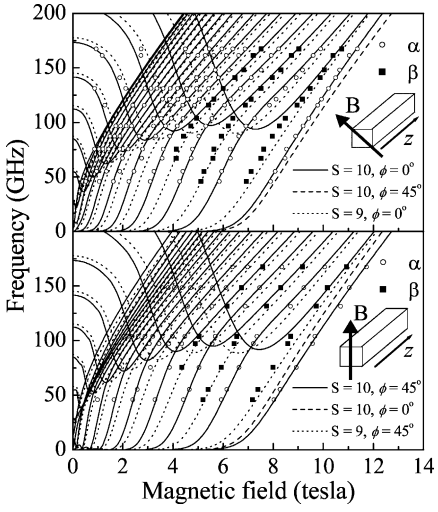

Fig. 8. Fits to Mn_{12}-Ac (sample C) hard axis data for the two orientations within the hard magnetic plane ($\phi = 0$ and 45°). The solid squares and open circles represent two different series of resonances, labeled α and β according to the scheme adopted in our original investigations of Mn_{12}-Ac [4]. The α resonances fit the $S = 10$ model (solid curves) extremely well, and the obtained parameters, to fourth order, are listed in Table 1. The β resonances deviate from the $S = 10$ theory at low frequencies; a possible connection to the $S = 9$ state (dotted curves) is discussed in a separate publication [30]. The differences between the fits for the two orientations is due to the significant B_4^4 term (see Table 1); the dashed curve in each figure is included as a means for comparing the two orientations. The insets indicate the orientations of the applied field relative to the geometry of the sample—see main text for explanation.

4. Summary and conclusions

We review a wide body of recent single crystal EPR experiments which we have carried out on the Fe_8Br and Mn_{12}-Ac SMMs. These studies highlight important new aspects of the couplings between SMMs and their environment. We examine quantitatively the temperature dependence of the EPR linewidths and line shifts for fixed frequency measurements with an applied magnetic field along the easy axis. Simulations of the obtained experimental data take into account various couplings, including intermolecular spin–spin interactions (dipolar and exchange), as well as distributions in the zero-field crystal field parameters. Our results for Fe_8Br are the first to demonstrate significant intermolecular exchange interactions in this widely studied SMM. For Mn_{12}-Ac, a pronounced modulation of the EPR lineshapes for transverse applied fields likely confirms the solvent-disorder-induced transverse anisotropy model which has recently been proposed by other groups [20]. These findings could have important implications for the mechanism of quantum tunneling of magnetization in both of these SMMs, as well as providing deeper insights into the interactions which give rise to quantum decoherence.

Acknowledgements

We thank George Christou, David Hendrickson, Andrew Kent, Philip Stamp and Wolfgang Wernsdorfer for stimulating discussion. Funding is provided by the National Science Foundation (DMR 0103290 and DMR0196430) and by Research Corporation.

References

[1] G. Christou, D. Gatteschi, D.N. Hendrickson, R. Sessoli, MRS Bull. 25 (11) (2000) 66.
[2] M.N. Leuenberger, D. Loss, Nature 410 (2001) 789.
[3] A.L. Barra, D. Gatteschi, R. Sessoli, Phys. Rev. B 56 (1997) 8192.
[4] S. Hill, J.A.A.J. Perenboom, N.S. Dalal, T. Hathaway, T. Stalcup, J.S. Brooks, Phys. Rev. Lett. 80 (1998) 2453.
[5] I. Mirebeau, M. Hennion, H. Casalta, H. Andres, H.U. Güdel, A.V. Irodova, A. Caneschi, Phys. Rev. Lett. 83 (1999) 628.
[6] R. Caciuffo, G. Amoretti, A. Murani, R. Sessoli, A. Caneschi, D. Gatteschi, Phys. Rev. Lett. 81 (1998) 4744.
[7] A.-L. Barra, D. Gatteschi, R. Sessoli, Chem. Eur. J. 6 (2000) 1608.
[8] S. Maccagnano, R. Achey, E. Negusse, A. Lussier, M.M. Mola, S. Hill, N.S. Dalal, Polyhedron 20 (2001) 1441.
[9] S. Hill, S. Maccagnano, K. Park, R.M. Achey, J.M. North, N.S. Dalal, Phys. Rev. B 65 (2002) 224410.
[10] K. Park, M.A. Novotny, N.S. Dalal, S. Hill, P.A. Rikvold, Phys. Rev. B 65 (2002) 014426.
[11] K. Park, M.A. Novotny, N.S. Dalal, S. Hill, P.A. Rikvold, Phys. Rev. B 66 (2002) 144409.
[12] S. Hill, R.S. Edwards, J.M. North, K. Park, N.S. Dalal, Phys. Rev. Lett. (2003), accepted for publication; also cond-mat/0301599.
[13] E.M. Chudnovsky, J. Tejada, Macroscopic Quantum Tunneling of the Magnetic Moment, Cambridge University Press, Cambridge, 1998.
[14] (a) J.R. Friedman, M.P. Sarachik, J. Tejada, R. Ziolo, Phys. Rev. Lett. 76 (1996) 3830;
(b) L. Thomas, F. Lionti, R. Ballou, D. Gatteschi, R. Sessoli, B. Barbara, Nature (Lond.) 383 (1996) 145.
[15] C. Sangregorio, T. Ohm, C. Paulsen, R. Sessoli, D. Gatteschi, Phys. Rev. Lett. 78 (1997) 4645.
[16] W. Wernsdorfer, A. Caneschi, R. Sessoli, D. Gatteschi, A. Cornia, V. Villar, C. Paulsen, Phys. Rev. Lett. 84 (2000) 2965.
[17] J.R. Friedman, M.P. Sarachik, R. Ziolo, Phys. Rev. B 58 (1998) R14729.
[18] E. del Barco, A.D. Kent, E. Rumberger, D. Hendrickson, G. Christou, Europhys. Lett. 60 (2002) 768.
[19] K.M. Mertes, Y. Suzuki, M.P. Sarachik, Y. Paltiel, H. Shtrikman, E. Zeldov, E. Rumberger, D.N. Hendrickson, G. Christou, Phys. Rev. Lett. 87 (2001) 227205.
[20] A. Cornia, R. Sessoli, L. Sorace, D. Gatteschi, A.L. Barra, C. Daiguebonne, Phys. Rev. Lett. 89 (2002) 257201.
[21] R. Amigó, E. del Barco, L.l. Casas, E. Molins, J. Tejada, I.B. Rutel, B. Mommouton, N. Dalal, J. Brooks, Phys. Rev. B 65 (2002) 172403.
[22] B. Parks, J. Loomis, E. Rumberger, D.N. Hendrickson, G. Christou, Phys. Rev. B 64 (2001) 184426.
[23] (a) D.A. Garanin, E.M. Chudnovsky, Phys. Rev. B 65 (2002) 094423;
(b) E.M. Chudnovsky, D.A. Garanin, Phys. Rev. Lett. 87 (2001) 187203.
[24] M. Mola, S. Hill, M. Gross, P. Goy, Rev. Sci. Instrum. 71 (2000) 186.
[25] T. Lis, Acta Crystallogr. B 36 (1980) 2042.
[26] K. Wieghart, K. Pohl, I. Jibril, G. Huttner, Angew. Chem., Int. Ed. Engl. 23 (1984) 77.
[27] W. Wernsdorfer, N. Aliaga-Alcalde, D.N. Hendrickson, G. Christou, Nature 416 (2002) 406–409.
[28] W. Wernsdorfer, S. Bhaduri, R. Tiron, D.N. Hendrickson, G. Christou, cond-mat/0206195, unpublished.
[29] R.S. Edwards, S. Hill, S. Bhaduri, N. Aliaga-Alcade, E. Bolin, S. Maccagnano, G. Christou, D.N. Hendrickson, these proceedings.
[30] R.S. Edwards, S. Hill, S. Maccagnano, J.M. North, N.S. Dalal, cond-mat/0302052.